Water versus DNA: new insights into proton track-structure modelling in radiobiology and radiotherapy

2015 Phys. Med. Biol. 60 7805

(http://iopscience.iop.org/0031-9155/60/20/7805)

IOP Publishing | Institute of Physics and Engineering in Medicine Physics in Medicine & Biology

Phys. Med. Biol. **60** (2015) 7805–7828 doi:10.1088/0031-9155/60/20/7805

Water versus DNA: new insights into proton track-structure modelling in radiobiology and radiotherapy

C Champion[1], M A Quinto[2], J M Monti[2], M E Galassi[2], P F Weck[3], O A Fojón[2], J Hanssen[2] and R D Rivarola[2]

[1] Université de Bordeaux, CNRS/IN2P3, Centre d'Etudes Nucléaires de Bordeaux Gradignan, Gradignan, France
[2] Instituto de Física Rosario, CONICET and Universidad Nacional de Rosario, Rosario, Argentina
[3] Sandia National Laboratories, Albuquerque, NM 87185, USA

E-mail: champion@cenbg.in2p3.fr

Received 4 April 2015, revised 10 June 2015
Accepted for publication 24 June 2015
Published 25 September 2015

Abstract

Water is a common surrogate of DNA for modelling the charged particle-induced ionizing processes in living tissue exposed to radiations. The present study aims at scrutinizing the validity of this approximation and then revealing new insights into proton-induced energy transfers by a comparative analysis between water and realistic biological medium. In this context, a self-consistent quantum mechanical modelling of the ionization and electron capture processes is reported within the continuum distorted wave-eikonal initial state framework for both isolated water molecules and DNA components impacted by proton beams. Their respective probability of occurrence—expressed in terms of total cross sections—as well as their energetic signature (potential and kinetic) are assessed in order to clearly emphasize the differences existing between realistic building blocks of living matter and the controverted water-medium surrogate. Consequences in radiobiology and radiotherapy will be discussed in particular in view of treatment planning refinement aiming at better radiotherapy strategies.

Keywords: proton transport, cross sections, energy transfers, water and DNA, radiobiology, radiotherapy

(Some figures may appear in colour only in the online journal)

1. Introduction

In the context of biomolecular radiation damage, primary charged particles loose energy during interaction with biological tissues, potentially leading to the creation of secondary electrons in the medium. Modelling the radiobiological damages induced by such ionizing particles crossing the living matter requires a precise knowledge of the full radiation history, including the energy deposited during inelastic collisions as well as the kinetic energy transferred to secondary particles eventually emitted.

In order to capture the complexity of the biological radiation damage induction mechanism at the molecular level, it is of prime importance to quantify the full kinematics of the main ionizing processes. Monte-Carlo (MC) track structure codes are among the best-suited tools to achieve that goal since they provide an adequate description of the radio-induced energetic pattern at the finest scale, i.e. at the cellular or sub-cellular level [see (Nikjoo *et al* 2006) for a review]. However, the reliability of such numerical methods heavily depends on the accuracy of the input data used in the simulations, namely, the interaction cross sections needed for describing the various collisional processes involved in the slowing-down of the charged particles in the medium of interest. For that reason, a precise description of the most important ionizing interactions i.e. the ionization and the electron capture processes is of crucial importance in proton track-structure modelling.

Drawing up an exhaustive list of models implemented into the MC codes documented in the literature would be a daunting task in view of the variety of existing approaches, which include theoretical, semi-empirical as well as experimental approaches. For more details, we refer the reader to our previous works where a comparison between measurements and theoretical/semi-empirical predictions was given for proton-induced ionization and capture in water vapour (Champion *et al* 2013, Rivarola *et al* 2013) as well as the series of works based on the dielectric response function for describing the charged particle induced interactions in liquid water (see for example the recent work of Dingfelder (2014) and the review provided by Emfietzoglou *et al* (2013)). Nevertheless, from a general standpoint, the predictive power of such models remains either restricted to the domain of validity of the theoretical approximations used or limited by the availability of the experimental data. Regarding the latter, of course we essentially find total cross sections, the multiple differential cross sections—needed to describe the angular and the energetic distributions of the secondary emitted electrons—being indeed rarely measured due to the complexity of simultaneous energetic and angular detection. Therefore, semi-empirical laws are usually preferred in the proton transport numerical simulations, although the paucity of measured data may sometimes lead to questionable results largely based on extrapolations.

In order to address such shortcomings, we recently proposed a series of quantum-mechanical models based on the first-Born approximation with correct boundary conditions (CB1 model) and the continuum distorted wave-eikonal initial state (CDW-EIS) methodology to describe the proton-induced ionization and electronic capture in water vapour (Champion *et al* 2013, Rivarola *et al* 2013). In brief, the CB1 model describes the active (ejected) electron as being in bound and continuum states of the target field in the entry and exit collision channels, respectively, while the CDW-EIS description gives a more 'complete' representation of the active electron, considering that it evolves in the *simultaneous* presence of both the projectile and target fields in the entry and exit channels at all collision times. In this way, the CB1 model is commonly referred to as a *one-centre* approach and the CDW-EIS model as a *two-centre* one. Furthermore, correct boundary conditions were considered in the CB1 and CDW-EIS models, meaning that asymptotic Coulomb long-range interaction between the projectile and the active electron was accounted for in the initial and final wave functions.

Both CB1 and CDW-EIS models are valid for high enough collision energies, namely, for impact energies greater than about 50 keV amu^{-1}. In fact, the CDW-EIS model was originally introduced to give a better description than the one-centre models of both the ionization (Crothers and McCann 1983) and capture (Martínez *et al* 1988) processes, in particular in the intermediate impact energy regime i.e. where the impact velocity is comparable to the initial electron orbital velocity. Thus, for water vapour we have tested that the CDW-EIS model gives an adequate description in terms of total and differential cross sections of both the ionization and the electron capture processes for impact energies of the order of a few tens of keV. Similarly, we have shown that the CB1 predictions exhibit an overall good agreement with the experiment provided that the impact energy is greater than about 100 keV amu^{-1} (Champion *et al* 2013, Rivarola *et al* 2013).

Recently, both quantum-mechanical models were extended to handle more complex molecular targets and thoroughly tested in a series of studies dedicated to the description of the proton-induced ionization and electron capture on DNA/RNA components. Molecular structure information for the biological targets of interest was provided by *ab initio* calculations [see (Galassi *et al* 2012) for details]. Total, single- and double-differential ionization cross sections were calculated within the CB1 and CDW-EIS approximations and compared to a large set of experimental data for protons, α-particles, carbon and fluorine ion beams impacting on the various DNA/RNA compounds, including the nucleobases (adenine (A), cytosine (C), thymine (T), guanine (G) and uracil (U)) and the sugar-phosphate (SP) backbone (Champion *et al* 2010, Agnihotri *et al* 2012, 2013a, 2013b, Galassi *et al* 2012, Itoh *et al* 2013). Similarly, the electron capture process was investigated by means of two continuum distorted wave models (CDW and CDW-EIS) and a comparison between theoretical predictions and scarce experimental data was reported in (Champion *et al* 2012).

These pioneer studies were particularly important since in the vast majority of existing numerical simulations devoted to radio-induced damage modelling and its numerous derivatives (radiotherapy, dosimetry, medical imaging…), the biological environment is usually modelled by water, which accounts for more than 50–80 wt% in the cellular environment, depending on the age of the patient. However, it is nowadays well known that the history of any charged particle in matter and, consequently, the energy deposit pattern are sensitive to the nature of the molecules impacted. Therefore, it can be inferred that using cross sections of water instead of realistic cross sections in track-structure simulations may lead to an underestimation of the DNA radiation damages (strand breaks, base lesions…), as already suggested by many authors [see e.g. (Rabus *et al* 2014)]. Moreover, many groups have demonstrated in the past that the role played by the DNA components—and more particularly by the terminal phosphate group and the base moieties—might be crucial in the radio-induced damage distribution in particular for *direct* action of low-energy electrons [see, e.g. the series of works provided by Sanche and co-workers (Zheng *et al* 2005, Li *et al* 2008, 2010)].

The current work aims at scrutinizing the appropriateness of water as a surrogate for modelling the main ionizing proton-induced processes in human tissue and revealing new insights into proton-induced energy transfers in realistic biological medium. The biomolecular targets under investigation are considered as *isolated* molecules and then refer to living matter components in vapour state. In this sense, the present work clearly differs from the existing studies on *condensed* DNA where the energy-loss function of realistic biological components was extracted from experimental data and interpolated for being used in cross section calculations [see for example the series of works provided by Abril and co-workers (Abril *et al* 2011, de Vera *et al* 2015)].

The objective is here to provide an *intra comparison* of the two major collisional processes in water versus DNA, each target being modelled within the same approximation. Under these

conditions, a self-consistent quantum mechanical modelling of the ionization and electron capture processes in water and DNA is here reported, within the aforementioned CDW-EIS framework, for both *isolated* water molecules and DNA components impacted by protons. Their respective probability of occurrence—expressed in terms of total cross sections—as well as their energetic signature are assessed in order to emphasize the differences existing between realistic building blocks of living matter and the controverted water-medium surrogate.

Finally, let us add that even if the investigated targets are described in vapour phase, we obviously consider a density scaling when we investigate the radiobiological and medical applications in the last section of this work.

2. Methodology

2.1. Biological matter description

The input parameters used for describing the occupied molecular orbitals (MOs) of the biomolecular targets here investigated were obtained by using an *ab initio* method in which each molecular orbital was described by a linear combination of atomic wave functions by using the GAUSSIAN09 software at the RHF/3-21G level (Frisch *et al* 2009). The equilibrium geometries of the nucleobases were obtained without symmetry constraints applied, whereas the structure of the SP backbone unit was optimized following the procedure suggested by Colson *et al* (1993) for a typical B-DNA fiber conformation. The resulting first ionization potential of the backbone unit was 10.53 eV, in close agreement with the scaled value of 10.52 eV obtained by Bernhardt and Paretzke (2003), while the computed ionization energies of the occupied molecular orbitals of the nucleobases were scaled so that their calculated Koopmans ionization energy, i.e. the ionization energy of their HOMO coincides with the experimental value of the ionization potential measured by Hush and Cheung (1975). Besides, the effective number of electron relative to the atomic component was derived from a standard Mulliken population analysis. For more details, we refer the interested reader to our previous study (Galassi *et al* 2012) where all the quantum numbers and coefficients needed for expressing the target molecular wave functions are reported.

2.2. Cross section calculation

The reactions of interest are here the single electron capture and the single electron ionization processes induced by impact of bare ions on molecular targets. Due to the complexity of such multi-electron processes, we first reduced the current problem to the study of a three-body system composed by the projectile, the active electron and the residual target [for more details, we refer the reader to the original works given by Corchs *et al* (1993) and by Galassi *et al* (2004) which refer to the first descriptions of the electron capture and ionization from molecular targets, respectively]. Besides, the passive electrons (the not captured or ionized ones) are assumed to remain in their respective bound orbital during the collision. Let us note that this second approximation is valid at high enough impact energies i.e. when the collision time is smaller than the relaxation time of the passive electrons as well as the vibrational and rotational ones. In addition, due to the large difference between the proton mass and that of the target electron, the straight-line version of the impact parameter approximation is employed for describing both the ionization and the electron capture processes.

Within this independent active electron approximation, the interaction of the projectile nucleus with the passive electrons is averaged over the orbital distributions of the latter ones.

As a consequence, it appears in the Hamiltonian as a static potential depending of the distance of the projectile to the center of mass of the molecular target. Thus, its influence on the initial and final wave functions in the entry and exit channels, respectively, appears under the form of an exponential factor with a purely imaginary argument, as it happens for the interaction between the projectile nucleus and all the nuclei of the molecule. It can then be shown that both exponential factors do not affect the electronic transition when integration over all projectile scattering distributions is performed (Corchs *et al* 1993, Galassi *et al* 2004). This is the case of our present interest since differential cross sections only depending on the final electronic energy and/or angular distributions are presented for electron ionization. Besides, for electron capture only total cross sections are calculated. Thus, the interactions of the projectile with the residual target can be excluded from the present analysis. Under these conditions, the Hamiltonian describing the evolution of the active electron is reduced to the expression

$$H_{\mathrm{el}} = -\frac{\nabla^2}{2} - \frac{Z_P}{s} - V_T(\mathbf{x}) \tag{1}$$

where it has been considered that the electronic mass is much more smaller that the projectile and the residual target ones.

In the above expression, Z_P is the projectile nuclear charge, $\mathbf{x}$ and $\mathbf{s}$ are the position vectors of the active electron with respect to the center of mass of the molecular target and to the projectile nucleus, respectively, while $V_T(\mathbf{x})$ refers to a potential describing the influence of the residual target on the active electron, containing thus the interaction of the active electron with the target nuclei and the passive electrons.

In the α-entry channel, the initial one-active electron distorted wave function is chosen as

$$\chi_\alpha^+ = \varphi_\alpha(\mathbf{x}) \exp(-\mathrm{i}\varepsilon_\alpha t) L_\alpha(\mathbf{s}) \tag{2}$$

where the super-index $(+)$ indicates the outgoing character of the distorted wave function whereas $\varphi_\alpha(\boldsymbol{x})$ represents the non-perturbed initial electron bound orbital and ε_α its orbital energy.

The L_α distortion factor is given by

$$L_\alpha(\mathbf{s}) = \exp[-\gamma v \ln(vs + \mathbf{v}\cdot\mathbf{s})] \tag{3}$$

where γ is defined as $\gamma = \frac{Z_P}{v}$ with v the impact velocity. As the distorted function included in the entrance channel depends on the $\mathbf{s}$ coordinate, it takes into account the fact that the electron bound to the target is simultaneously at all collision times in a continuum state of the projectile field, being the latter considered through an eikonal approximation. It gives a two-center character to the distorted wave function. Moreover, the Coulomb behavior of the projectile field at long distances s is contained in the initial distorted wave function in the entry α-channel, preserving thus correct boundary conditions at collision times $t \to -\infty$ ($t = 0$ corresponding to the closest approach of the projectile to the target for each given impact parameter). The simple choice of a multiplicative continuum distorting factor has as a consequence that the potentials $(-Z_p/s)$ and V_T do not appear in the initial perturbation potential W_α, which results from the time-dependent Schrödinger equation $\left(H_{el} - i\frac{\partial}{\partial t}\right)\chi_\alpha^+ = W_\alpha \chi_\alpha^+$.

For electron capture, the final wave function in the β-exit channel is chosen as

$$\begin{aligned}\chi_\beta^- = {} & \varphi_\beta(\mathbf{s}) \exp(-i\varepsilon_\beta t + i\mathbf{v}\cdot\mathbf{x} - iv^2 t/2) \\ & \times N(\varsigma)\, {}_1F_1(-i\varsigma; 1; -ivx - i\mathbf{v}\cdot\mathbf{x})\end{aligned} \tag{4}$$

where $\varphi_\beta(\mathbf{s})$ represents the final non-perturbed bound projectile state and ε_β its corresponding orbital energy.

In equation (4), ${}_1\mathrm{F}_1(-\mathrm{i}\,\varsigma;\,1;\,-\mathrm{i}\,v\,x-\mathrm{i}\,\boldsymbol{v}\cdot\boldsymbol{x})$ refers to the Coulomb continuum factor related to the electron-residual target interaction where $\varsigma = Z_T^*/v$ with Z_T^* an effective target nuclear charge defined by $Z_T^* = \sqrt{-2n^2\varepsilon_\alpha}$ where the value of n is equal to the principal quantum number of each atomic orbital used to describe the molecular orbitals.

In order to simplify the calculations associated with the use of a target numerical continuum factor, the interaction between the active electron and the residual target has been approximated by an effective Coulomb potential, in such a way that $V_T \cong V_T^* = -Z_T^*/x$. This approximation limits the description of correct boundary conditions associated with the V_T potential in the exit channel at asymptotic long distances x but privileges the region where electron capture reaction is produced. Moreover, asymptotic boundary conditions are satisfied for the approximated Hamiltonian resulting by replacing V_T by V_T^*.

In equation (4), the function $N(a) = \exp(\pi a/2)\Gamma(1-\mathrm{i}a)$ gives the normalization of the corresponding continuum factor. The final distorted wave-function presents also a two-centre character associated with the fact that the electron evolves in the combined field of the projectile and residual target. Now, the super-index $(-)$ indicates that correct ingoing conditions are satisfied.

For ionization, the final distorted wave function is taken as

$$\begin{aligned}\chi_\beta^- = {} & (2\pi)^{-3/2}\exp(-i\varepsilon_\beta t + i\mathbf{k}\cdot\mathbf{x} - ik^2t/2)\\ & \times N^*(\xi)\,{}_1F_1(-i\xi;\,1;\,-ikx - i\mathbf{k}\cdot\mathbf{x})\\ & \times N^*(\zeta)\,{}_1F_1(-i\zeta;\,1;\,-ips - i\mathbf{p}\cdot\mathbf{s})\end{aligned} \tag{5}$$

where $\mathbf{k}$ and $\mathbf{p} = \mathbf{k} - \mathbf{v}$ are the linear momenta of the electron with respect to the target and projectile nucleus, respectively.

Finally, let us remind that the Sommerfeld parameters ξ and ζ are defined by $\xi = Z_T^*/k$ and $\zeta = Z_P^*/p$. In the rhs of equation (5), the functions depending on the $\mathbf{x}$ coordinate describe the electron in a continuum state of the residual target (represented by an effective Coulomb field) whereas the continuum factor depending on the coordinate $\mathbf{s}$ corresponds to the electron-projectile interaction. Thus, the final distorted wave function describes the electron travelling simultaneously in a continuum state of both the projectile and the residual target fields, and their actions on the emitted electron are considered on equal footing.

Once more, it must be noted that the distorted wave function χ_β^- for ionization presents the asymptotic behavior

$$\chi_\beta^- \xrightarrow[x,s\to+\infty]{} (2\pi)^{-3/2}\exp(-\mathrm{i}\varepsilon_\beta t + \mathrm{i}\mathbf{k}\cdot\mathbf{x} - \mathrm{i}k^2t/2)\times\left[\mathrm{i}\frac{Z_T^*}{k}\ln(kx+\mathbf{k}\cdot\mathbf{x}) + \mathrm{i}\frac{Z_P}{p}\ln(ps+\mathbf{p}\cdot\mathbf{s})\right] \tag{6}$$

The *post* and *prior* versions of the transition amplitude for the reactions above mentioned may be written as

$$A_{\alpha,\beta}^+ = -i\int_{-\infty}^{+\infty} dt\left\langle \chi_\beta^-\left|\left(H_{el} - i\frac{\partial}{\partial t}\right)^\dagger\right|\chi_\alpha^+\right\rangle \tag{7}$$

$$A_{\alpha,\beta}^- = -i\int_{-\infty}^{+\infty} dt\left\langle \chi_\beta^-\left|\left(H_{\mathrm{el}} - i\frac{\partial}{\partial t}\right)\right|\chi_\alpha^+\right\rangle \tag{8}$$

respectively, with H_{el} the electronic Hamiltonian.

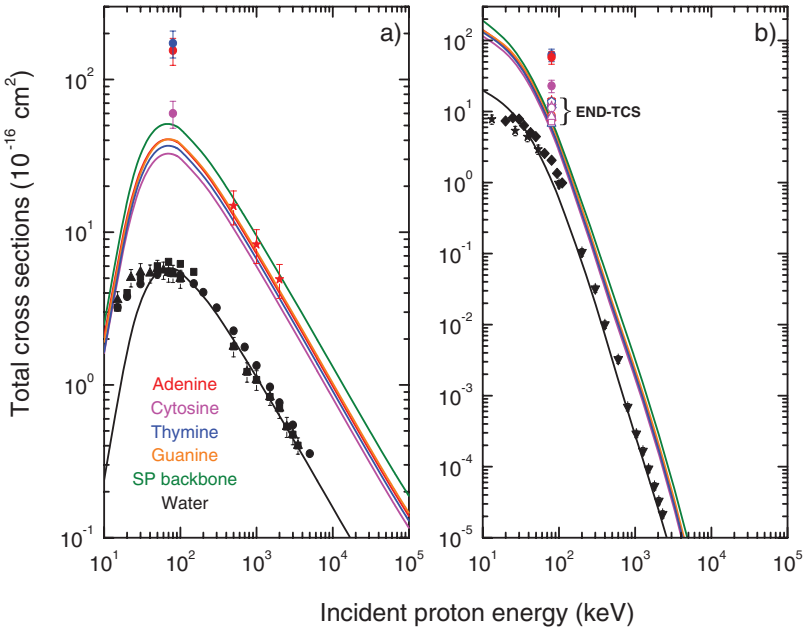

Figure 1. (Colour online) Total cross sections (per target) for proton impacting on water molecule (black lines and symbols) and DNA components (color lines and symbols): (a) ionization process—(b) electron capture process. The experimental data are taken from Luna *et al* (2007) (up-triangles), Bolorizadeh and Rudd (1986) (squares), Rudd *et al* (1985) (circles), Gobet *et al* (2001) (diamonds), Dagnac *et al* (1970) (stars) and Toburen (1998) (down-triangles) for proton-induced ionization and capture in water. For DNA components, experimental TCS are taken from Iriki *et al* (2011a, 2011b) for A ionization and from Tabet *et al* (2010) for A, C and T ionization and capture. The theoretical cross sections provided by Privett and Morales within the END framework (Privett and Morales 2014) are also reported for comparison (open symbols).

In the current work, the cross sections for electron capture are computed within *prior* version whereas for electron ionization the *post* version is used for simplicity (Champion *et al* 2010, 2012, Galassi *et al* 2012).

3. Results and discussion

3.1. Interaction cross sections

The total cross sections (per target) for proton impacting on isolated water molecules and DNA components are reported for ionization and electron capture in figures 1(a) and (b), respectively. We clearly observe that the CDW-EIS model reproduces very well the experimental measurements of water vapour (for ionization and capture) for proton incident energies greater than ~50 keV, while the low-energy domain is, as expected, largely overestimated. Regarding the DNA nucleobases and the SP backbone, a large degree of similarity is observed among all the components considered. Besides, the present theoretical predictions show a very good agreement with the experimental data recently reported by Iriki *et al* (2011a, 2011b) for 0.5-, 1- and 2 MeV protons impacting on adenine targets. On the other hand, the data reported by Tabet *et al* (2010) at 80 keV exhibit large discrepancies with our results (by a factor of ~2–5

Table 1. Total cross sections (expressed in 10^{-16} cm^2 units) for 80 keV-proton-induced electron capture in A, C and T targets. Comparison between the current CDW-EIS values, the theoretical predictions provided by Privett and Morales within the END framework by using various basis sets [see Privett and Morales (2014) for more details] and the experimental data reported by Tabet *et al* (2010).

	Experimental data	Current CDW-EIS model	END model			
			STO-3G	3-21G	6-31G	6-31G/ $H^+ + +^{**}$
Adenine (A)	58 ± 12	5.9	13.9	8.8	8.1	12.5
Cytosine (C)	23 ± 5	5.1	12.1	7.9	7.3	11.2
Thymine (T)	63 ± 13	5.7	13.3	8.2	6.8	11.4

for ionization and of one order of magnitude for capture), a tendency, which has been recently confirmed by the calculations performed by Privett and Morales within the electron nuclear dynamics (END) framework (Privett and Morales 2014). In their work, the authors developed two independent END models coupled with various types of basis sets for describing the biomolecular targets and demonstrated the ability of their theories to accurately describe the one-electron transfer process for proton-induced collisions on A, C, T and U nucleobases. The results obtained are reported in figure 1(b) for comparison and show an overall good agreement with our theoretical predictions—even considering their dispersion relative to the basis set used—and clearly point out huge discrepancies with the measurements reported by Tabet and co-workers (see table 1).

Figure 1(a) shows that, regardless of the molecular target investigated, the ionization cross sections feature similar variations as functions of the incident energy, with in particular a maximum located around 70 keV. However, the amplitude of the 'DNA-components' cross sections is higher by a factor of 6–10 than that of the water molecule, a tendency that may also be observed for the capture process. This result is directly linked to the *total* number of target electrons since when normalized per target electron, i.e. 10 for water, 58 for C, 66 for T, 70 for A, 78 for G and 96 for the SP backbone, we obtain a 'universal' cross section, as seen in figure 2. Let us note that this suggests that the mean free path for protons in water will be similar to that in DNA (at constant density) and that « realistic » modelling the living matter, as opposed to using water cross sections, would have no effect on the transport simulation of protons in a non-homogeneous biological medium. However, this statement is only valid for *spatial* considerations; indeed, as demonstrated in the following, strong differences may arise in detailed analysis of the proton-induced *energy transfers* in water and DNA.

3.2. Energy transfers

Figure 3(a) depicts the average kinetic energy $\langle E_e \rangle$ transferred to secondary electrons during the ionization of each target investigated. The latter is calculated from the corresponding singly differential ionization cross sections, namely,

$$\langle E_e \rangle = \frac{\int E_e \frac{\mathrm{d}\sigma}{\mathrm{d}E_e} \mathrm{d}E_e}{\int \frac{\mathrm{d}\sigma}{\mathrm{d}E_e} \mathrm{d}E_e}. \tag{9}$$

The differences observed between water and DNA components remain small as long as the incident proton energy is low, i.e. below 100 keV, while noticeable discrepancies occur when

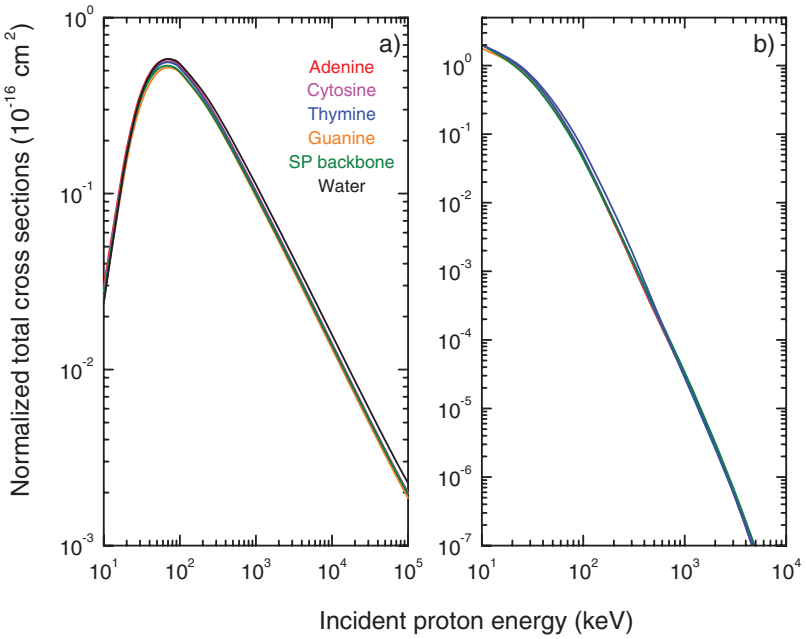

Figure 2. (Colour online) Normalized (per target electron) total cross sections: (a) ionization—(b) capture.

the proton energy increases. Besides, figure 3(a) exhibits an evident correlation between the amplitude of the average kinetic energy and the 'size' of the target, namely, the number of target electrons, as already observed in figure 1 in terms of total ionization cross sections. Thus, figure 3(a) shows that the minimal average kinetic energy of electrons extracted from DNA is attributed to cytosine (with 58 target electrons), the maximal energy being observed for the SP group (with 96 target electrons).

In this context, the kinetic energy released in water clearly appears lower than that of all the DNA components over the whole proton energy range. More precisely, at 10 MeV, figure 3(a) indicates that the average kinetic energy of the emitted electrons during the C ionization is 77.6 eV, i.e. 7% greater than for water (72.4 eV). For the SP backbone, the corresponding value is even higher, namely, 81.6 eV, i.e. 13% greater than for water. Finally, for the sake of comparison, the calculations provided by de Vera *et al* (2013) within the dielectric formalism (stars) have been also included in figure 3(a). A good agreement is observed over the whole proton energy range covered by the authors (10 keV–10 MeV).

Similarly, we report in the following the evolution of the deposited energy with respect to the proton energy for both ionization (figure 3(b)) and electron capture (figure 3(c)). This potential energy—related to ionization or capture—is calculated for each biomolecular target from the sum of all the corresponding partial (subshell) cross sections $\sigma_j = \sigma_j^{\text{ioniz}} + \sigma_j^{\text{capt}}$ weighted by the associated binding energy ($B_j = -\varepsilon_j$, see equation (2)), namely,

$$\left\langle E_{\text{dep}} \right\rangle = \frac{\sum_{j=1}^{N_{\text{MO}}} B_j \sigma_j}{\sum_{j=1}^{N_{\text{MO}}} \sigma_j} = \frac{\sum_{j=1}^{N_{\text{MO}}} B_j \sigma_j}{\sigma} \tag{10}$$

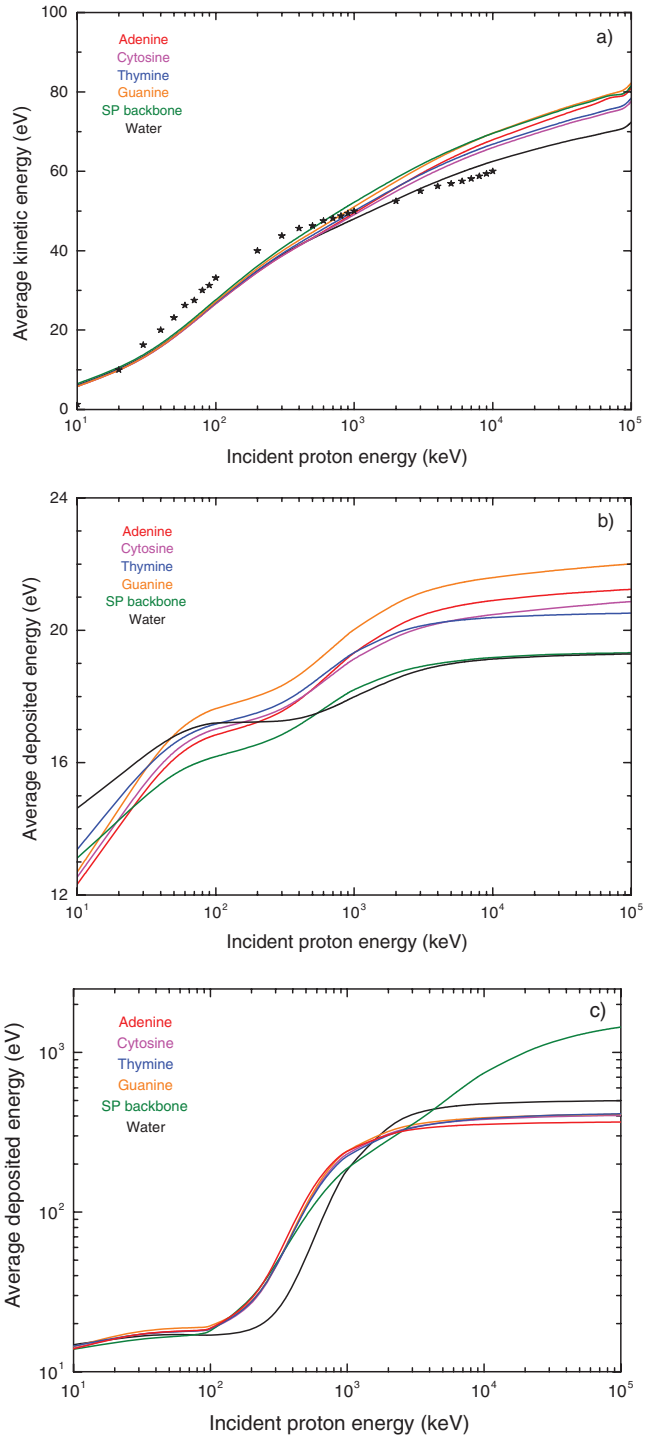

Figure 3. (Colour online) Average kinetic and deposited energies during proton-induced ionization and capture of water and DNA components. (a) Average kinetic energy of the secondary electrons; (b) average deposited energy during ionization; (c) average deposited energy during electron capture. The stars refer to the data reported by de Vera *et al* (2013).

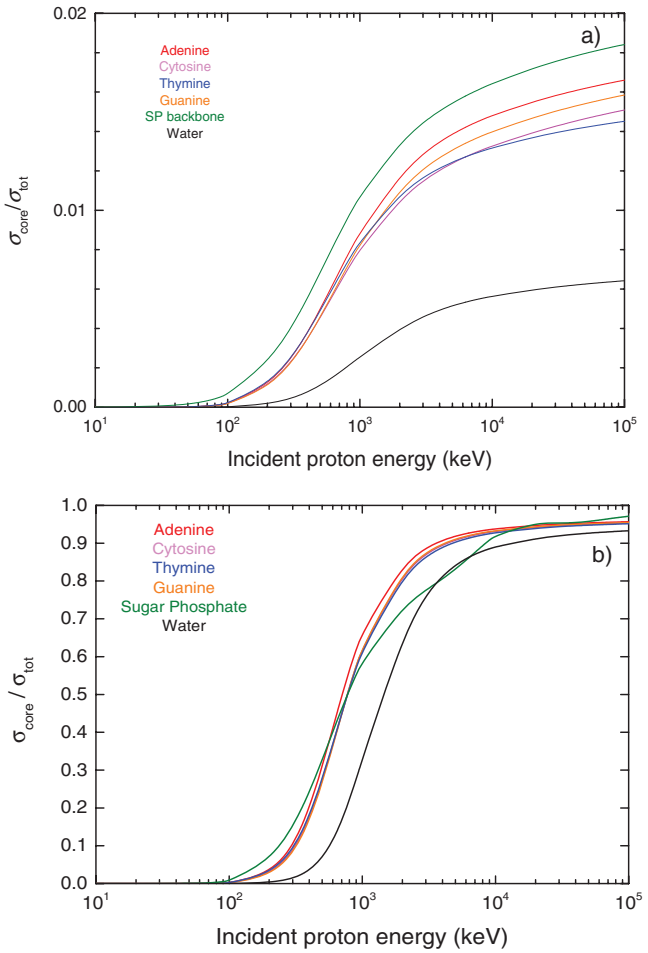

Figure 4. (Colour online) Contribution of the inner-shells into the ionization (panel a) and the electron capture (panel b) process for water and DNA components.

where N_{MO} refers to the number of molecular orbitals used in the description of each target ($N_{MO} = 5$ for water, 29 for C, 33 for T, 35 for A, 39 for G and 48 for the SP backbone) [see Galassi *et al* (2012) for details].

With regard to the ionization process (figure 3(b)), only slight differences may be observed between the different targets investigated, essentially due to the differences in magnitude of the binding energies involved into the ionization process. Nevertheless, the general tendency shows an asymptotic average deposited energy ranging from about 19 eV to 22 eV according to the DNA component, the water value being here again lower than that of all the DNA constituents and more particularly with the nucleobases. Indeed, from 1 MeV to 100 MeV proton-energy, the 'nucleobase group' shows a noticeable divergence with water ranging from 5–7% to 10–15% while the SP backbone asymptotically tends to about 19.32 eV i.e. very close to the water value (19.28 eV). In fact, this surprising result is linked to the combination of two factors, namely, (i) the relative contribution of the inner-shells into the ionization process, which is more important in the DNA case than in water (for all the components, as shown in figure 4(a)) and (ii) the inner-shell binding energies, which are of the same order of magnitude

for water and the nucleobases whereas they are about 4 times higher in the SP case, in particular due to the presence of the phosphate group. Consequently, the average energy deposited during the ionization of the inner-shells—expressed as the sum of the inner-shell cross sections weighted by the associated binding energy—shows a spectrum clearly dominated by the nucleobases in the high-energy regime (figure 3(b)).

On the other hand, in the case of the electron capture process the observations are quite different. Indeed, as can be seen in figure 3(c) where we have reported the evolution of the energy deposited during the electron capture process versus the proton energy, the water and the nucleobases show very similar contributions to the deposited energy pattern, the latter being in this case largely dominated by the SP backbone in the high-energy regime. Here again, the result has to be linked to the combined effects of the magnitude of the inner-shell binding energies and the inner-shell contribution to the capture process, which exhibits here a quasi-similar dependency with respect to the proton energy for all the targets (see figure 4(b)).

However, in the particular case of ionizing interaction on inner-shells, it is well known that the vacancy may be accompanied by the emission of an Auger electron that takes place at a short time scale after the interaction, typically between 0.001 and 5 fs. This Auger decay will necessarily modify the kinetic energy spectrum as well as the deposited energy pattern. Thus, by considering that all the inner-shell interactions are accompanied by an Auger relaxation process (regardless of the target investigated), we re-evaluated the average kinetic and potential energy spectra reported above. Specifically, the experimental value of 497.8 eV was used for the H_2O Auger electron energy (Siegbahn *et al* 1975) while semi-empirically estimates of the DNA Auger electron energies were extrapolated by using the binding energy gaps of the different atomic constituents involved in the biomolecular target description (Larkins 1977) as well as the binding energies of the molecular subshells of the targets under investigation (see Galassi *et al* 2012). Besides, let us add that we have here assumed that the Auger relaxation probability was equal to 1 whatever the target and the inner shells impacted are. This approximation may be seen as a first degree of approximation and 'more realistic' probabilities will be taken into account in our future works for modelling the various non-radiative transition channels.

The energy transfers obtained for both the ionization and the electron capture processes by taking into account the Auger cascade decay are displayed in figure 5.

In comparison to figure 3, we clearly observe that the average kinetic energies also revised (figure 5(a)) are slightly higher, the increase being all the more important when the proton energy increases; as discussed previously, this results from the increasing contribution of the inner-shell into the ionization process as the proton energy increases (as shown in figure 4(a)). In particular, at 10 MeV, the C and the SP backbone results show an increase of the average secondary electron energy of about 10 and 16%, respectively, in comparison to the water result.

Regarding the deposited energy spectrum, an appreciable decrease in both ionization and capture (see figures 5(b) and (c), respectively) is also seen. However, the difference between water and DNA components remains still noticeable, in particular for the capture occurring on the SP backbone where a ratio of ~6 is observed with water when Auger decays are taken into account.

From a radiobiological standpoint, it is nowadays admitted that the deposited energy stands as one of the most relevant quantities, whose amplitude may directly be linked to the radiation ability of DNA damaging. In this context, figure 5 clearly highlights the particularity of the SP backbone, which distinguishes from the 'water-nucleobase' group in particular in the high-energy domain via the electron capture process. These findings should undoubtedly have important knock-on effects in radiobiology—in particular for predicting the single and double

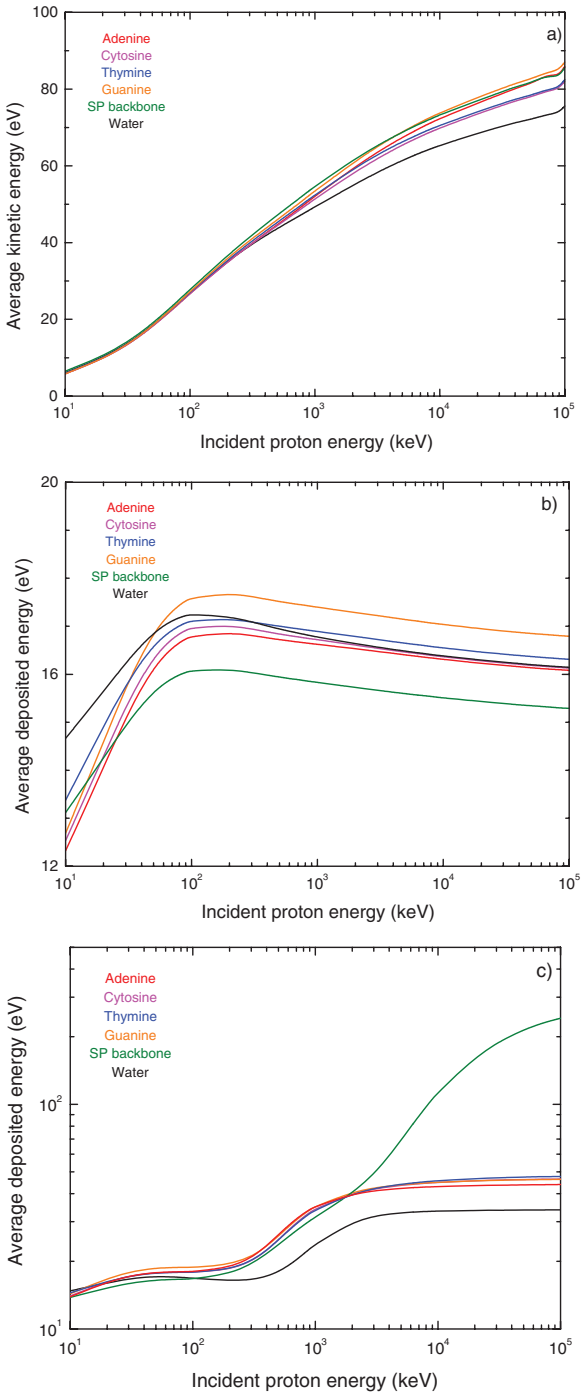

Figure 5. (Colour online) Revised average kinetic and deposited energies during proton-induced ionization and capture of water and DNA components here evaluated by taking into account the Auger process. (a) Average kinetic energy during ionization; (b) average deposited energy during ionization; (c) average deposited energy during electron capture.

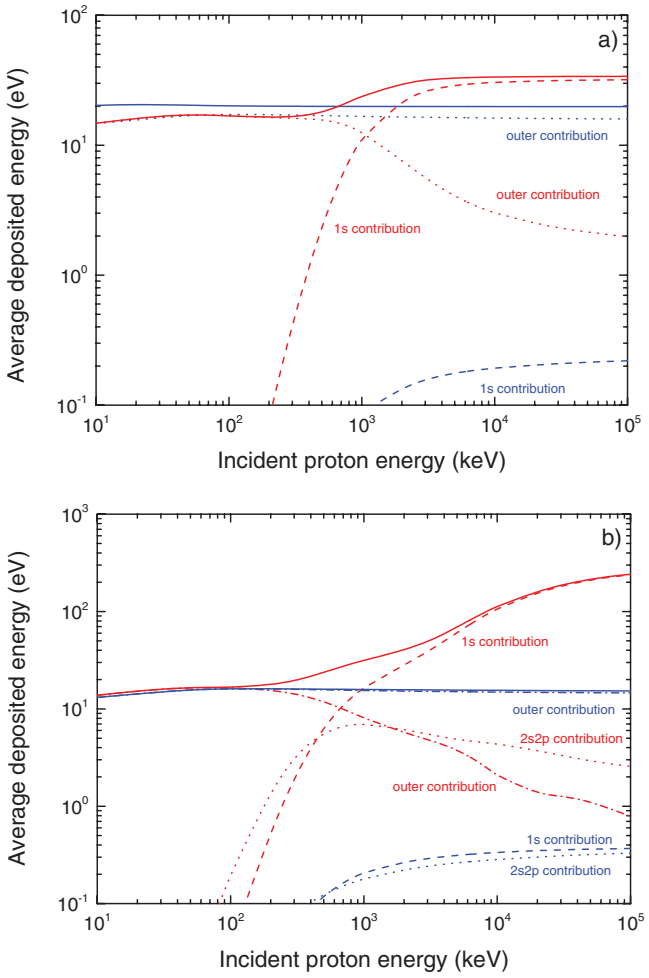

Figure 6. (Colour online) Detailed analysis of the energy deposit during proton-induced ionization and capture (blue and red line, respectively) for water (panel a) and desoxyribose-phosphate group (panel b). Note that the Auger process has been taken into account in the calculations.

strand break (SSB and DSB, respectively) induction—since the SP group is one of the main constituents of DNA involved in the macromolecule strand breakage.

In order to clearly appraise the specificity of this particular DNA element, we report in figure 6 a detailed comparison between water (panel a) and the SP group (panel b) in terms of energy deposit during the ionization and capture processes (blue and red line, respectively). Additionally, we separated the contribution of the inner subshells from the outer ones in both processes. Thus, as expected for ionization (blue lines), we observe that the main contribution arises from the outer shells (dash-and-dotted lines) for both water and SP group, leading then to a quasi-similar tendency with respect to the incident proton energy. On the other hand, with regards to the capture process (red lines)—which is characterized by a maximal probability of occurrence when the projectile velocity matches that of the target electron—figure 6 clearly points out the role played by the inner-shells, namely, the 1*s* contribution for both water and the SP group (dashed lines) and the 2*s*–2*p* contribution in the case of the SP group (dotted

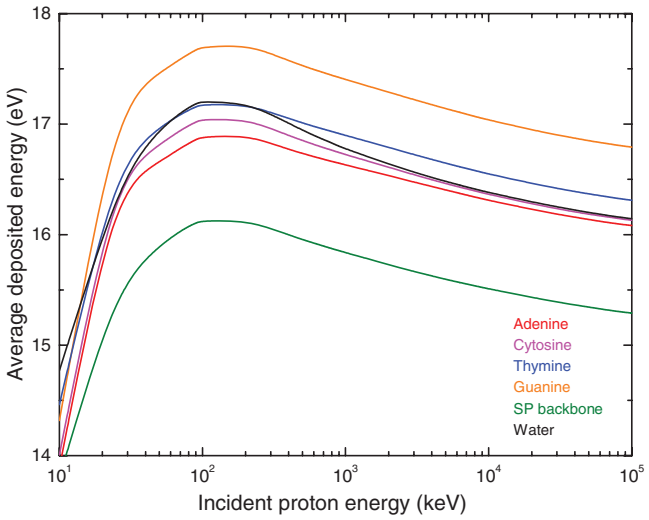

Figure 7. (Colour online) Average deposited energy per ionizing process for water and DNA components. Note that the Auger process has been taken into account in the calculations.

line). Thus, we observe that the inner-shell contribution dominates the global process provided that the proton energy is greater than about 1 MeV. These observations are noticeable for both water and the SP group. However, due to the large amplitude of the binding energies of the latter, the average energy deposited during an electron capture on the SP group largely exceeds that deposited in water.

From the energetic point of view, the differences of magnitude observed in figure 6 between water and the SP backbone clearly point out the crucial role of the SP, which is all the more important that it is nowadays well admitted that the two major sources of SSBs—which can be converted into potentially lethal DNA double-strand breaks if not repaired—are either the sugar or the nucleobase damage arising from primary radiation attack. However, many experimental studies have clearly demonstrated that among the various mechanisms of radiation damage induction, attacks on the SP backbone appears to be of the greatest importance and that attacks on bases are generally believed to not cause strand scission since arising indirectly, through enzymic removal of the damaged base by DNA base excision repair. Such reports have already been done by many experimental groups working on low-energy ion-induced damage to DNA building blocks who clearly shown that keV ion-induced DNA damages were largely dominated by deoxyribose disintegration [see e.g. (Deng *et al* 2005)].

However, let us not forget that the conclusions deduced from figure 6 are obtained by considering the two ionizing processes independently from each other i.e. without taking into account their relative probability of occurrence. Thus, if we are interested by the average energy deposit *per ionizing process*, i.e. without discriminating the collisional process, we have to weight up the above-reported values for ionization (figure 5(b)) and electron capture (figure 5(c)) by the corresponding total cross section (figure 1). In this case, we observe that all the targets exhibit quasi similar energy transfers—ranging from about 14 eV to 18 eV—the important role of the SP group having even disappeared, essentially due to the low probability of occurrence of the capture process in particular in the high-energy domain (see figure 7).

3.3. From isolated biomolecules to 'realistic' biological medium

In order to gain insight into the real energy deposit cartography induced by proton impact in biological medium, we have compared the mean energy deposit in water to its homologs in a 'realistic' DNA medium. To do that, we first considered a typical nucleotide i.e. an equivalent unit of DNA molecule composed of a nucleobase-pair plus two SP groups (La Verne and Pimblott 1995). Besides, to fit the realistic composition of living cells, we also took into consideration the nucleobase repartition percentages reported by Tan *et al* (2006), namely, 58% (A–T) (adenine–thymine base pair) and 42% (C–G) (cytosine–guanine base pair). Thus, by using the respective molar mass of each DNA component, namely, $M_A = 135.14\,g.mol^{-1}$, $M_T = 126.12\,g.mol^{-1}$, $M_C = 111.11\,g.mol^{-1}$, $M_G = 151.14\,g.mol^{-1}$ and $M_{SP} = 180\,g.mol^{-1}$, we obtained the following mass percentages: A (12.6%), T (11.8%), C (7.5%), G (10.2%) and SP group (57.9%).

However, this description refers to *dry* DNA, which obviously cannot intend to mimic the biological reality, mainly composed of hydrated DNA. Many studies have then shown that the mechanisms of degradation of DNA by direct energy deposition events were strongly dependent of the level of hydration of the nucleotide. Thus, Yokoya *et al* (2002) demonstrated that the yields of SSB's and DSB's slightly increased with respect to the level of hydration of DNA—from vacuum-dried DNA up to DNA containing 15 water molecules per nucleotide—the yields being constant at higher levels of hydration. The precise degree of hydration of macromolecules depends upon a variety of factors, including pH and concentration of salt in medium. Also, the value obtained varies with the method by which it is determined, some methods measuring only tightly bound molecules, while others also include water molecules more loosely associated with the macromolecule. Thus, Birnie *et al* (1973) estimated that the total amount of water associated with DNA was of the order of 50 moles per mole of nucleotide, in order to get the expected density of $1.29\,g.cm^{-3}$. Consequently, we also considered a biological medium composed of hydrated DNA here simulated by adding 18 molecules per nucleotide, that led to the following revisited mass percentages: A (8.3%), T (7.7%), C (4.9%), G (6.7%), SP group (38.1%) and water (34.3%). Figure 8 shows the average potential (panel a) and kinetic (panel b) energy transfers in the three cases here investigated, namely, water, dry DNA and hydrated DNA.

Thus, figure 8 shows that the energy deposited here again evaluated ***per ionizing process*** is roughly similar in all the three cases over the whole proton energy range while the kinetic energy transferred to secondary electrons is slightly underestimated (of about 10% at 100 MeV) when water is used as surrogate of the biological medium.

3.4. Radiobiological endpoints

Microdosimetry consists in quantifying the spatial and temporal distributions of radiation interactions in specific nano-size target volumes. Originally, the interaction of ionizing radiations with biological matter was analysed in terms of deposited energy in spherical or cylindrical nano-volumes mimicking pieces of DNA (double helix segments, nucleosomes or chromatin fiber). In this context, a well-accepted approach proposed by Goodhead *et al* (1994) consists in evaluating the absolute frequencies of energy depositions in typical cylindrical targets of DNA dimensions and then looking for energy and volume criteria that correlate with the biological efficiency of the radiation under investigation. Using this phenomenological model, the authors have shown that the predominant features of radiations could be considered in terms of classes of initial clustered damages of increasing severity (Nikjoo 2003) and then proposed a classification of clusters according to the energy deposited in specific targets. More precisely, the authors shown that events occurring in structured model targets representing

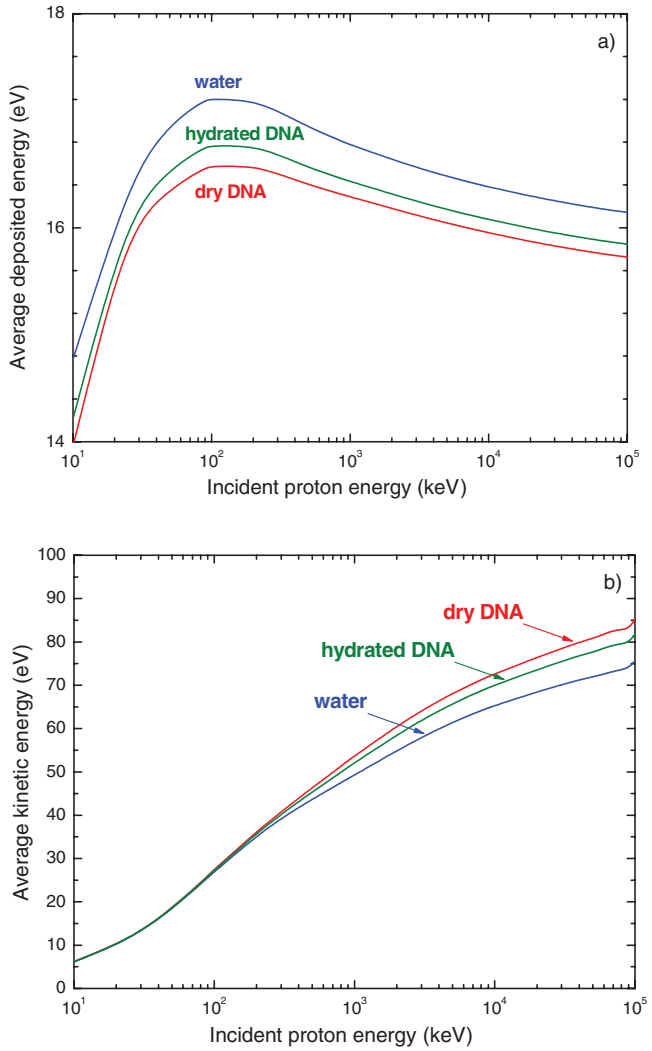

Figure 8. (Colour online) Average deposited energy (panel a) and kinetic energy (panel b) per ionizing process in water (blue) and 'realistic' biological medium (red: dry DNA, green: hydrated DNA). Note that the Auger process has been taken into account in the calculations.

DNA segment—typically cylinders of 2 nm-length and 2 nm-diameter—were correlated with the DNA single or double strand break induction (Nikjoo 2003). Since then, numerous numerical simulations of proton histories through biological matter were developed with the aim of scoring the energy deposit pattern and then identifying the energy threshold required for SSB and DSB induction (Nikjoo *et al* 1996). However, it goes without saying that the majority of existing numerical codes are based on the use of water as tissue-equivalent medium with—for the most sophisticated—the inclusion of the molecular DNA structure, which is finally superimposed on the ion track-structure in water (Friedland *et al* 1998). So, in view of the large above-reported discrepancies between water and DNA in terms of proton-induced energy deposit, we aim here at evaluating to which extent the energetic threshold commonly

suggested in the existing MC track-structure codes for predicting the DNA strand break induction [see Nikjoo *et al* (1999) for a review] should be revised if a more realistic description of the biological medium is used instead of water. It is beyond the scope of this study to discuss the consistency of the existing MC track-structure studies [for this purpose, we refer the interested reader the recent work of Pater *et al* (2014) who analysed the impact of the various user-defined parameters introduced into the direct radio-induced damage yields], and we only assess here the influence of the medium description on this energetic criteria whose quantification was semi-empirically deduced from comparisons between experiments and simulations in liquid water [see for example Nikjoo *et al* (1996) and Friedland *et al* (1998)]. To do so, the authors usually superimpose the energy deposit cartography simulated in liquid water on more or less complex models of the cellular environment [see for example Nikjoo *et al* (1996) and Friedland *et al* (1998, 2011) and Bernal *et al* (2013, 2015)].

Besides, let us remind that we consider here only the *proton*-induced interactions, what means that we do not account the contribution of the secondary electrons even considering that the latter are mostly responsible for DNA damage either by directly breaking the DNA strands or by producing reactive radicals during the water radiolysis, as demonstrated by many authors [see for example Nikjoo *et al* (2008)]. However, a complete modelling of these secondary electron histories would necessarily require the use of a Monte Carlo track structure code, what is out of the scope of the current theoretical study.

Under these conditions, we first calculated the mean number of interactions (ionizations + captures) $<N_{\text{int}}>$ induced by *proton* along a randomly positioned track segment crossing the critical cylinder volume of 2-nm-diameter by 2-nm-length. $<N_{\text{int}}>$ may be simply expressed by $<N_{\text{int}}> = <L> / \lambda$ where $<L>$ refers to the average path length through any randomly positioned cylinder while $\lambda \equiv \lambda(E_{\text{inc}})$ denotes the mean free path of an incident proton with energy E_{inc}. The latter is relied to the interaction cross section σ in the medium crossed by the incident proton (water or DNA) via the corresponding target density n, namely, $\lambda \equiv 1/n\sigma$. Thus, by using—***as a first attempt***—an equivalent mass density of 1 g cm^{-3} for all the three media investigated (water, dry DNA and hydrated DNA), we obtained the following target densities: $n_{\text{water}} = 0.033$ molecule Å^{-3}, $n_{\text{dryDNA}} = 0.96 \times 10^{-3}$ molecule Å^{-3} and $n_{\text{hydrated DNA}} = 0.63 \times 10^{-3}$ molecule Å^{-3}. Besides, the above-reported quantity $<L>$ is given by the Cauchy formula, which expresses the average path length for any straight particle track entering any convex or non-convex domain with isotropic uniform incidence. This latter is equal to $4V/S$ where V and S represent the volume and the surface of the body. Let us note that the average length of the trajectories depends only on the geometry of the system and is independent of the characteristics of the diffusion process as noted by Blanco and Fournier (Blanco and Fournier 2003). Considering then the dimensions of the target cylinder of interest in our study, namely, 2 nm-length and 2 nm-diameter, we obtained $<L> = 4/3$ nm and finally expressed the mean number of interactions as $<N_{\text{int}}> = (40/3)n\sigma$ with σ in Å^2. The mean energy deposited within the DNA-size cylinder $<E_{\text{dep}}>$ is finally expressed by the product of $<N_{\text{int}}>$ by the average deposited energy *per ionizing process* reported in figure 8(a).

The obtained results are plotted in figure 9. Whether it is in terms of interaction number or potential energy (figures 9(a) and (b), respectively), we clearly observe that considering water as the main component of DNA overestimates the biological reality. More precisely, for proton energies greater than about 100 keV the inset of figure 9(a) reports discrepancies in terms of interaction number of about 10–15% for hydrated DNA (green line) and 17–23% in dry DNA. Consequently, the deposited energy distribution exhibits a similar behavior (figure 9(b)) over the whole energy range and clearly highlights a large overestimation of the water-based predictions (>15%). These findings clearly indicate that the phenomenological parameters such as the energy threshold used for analysing the SSB and DSB induction in cells exposed

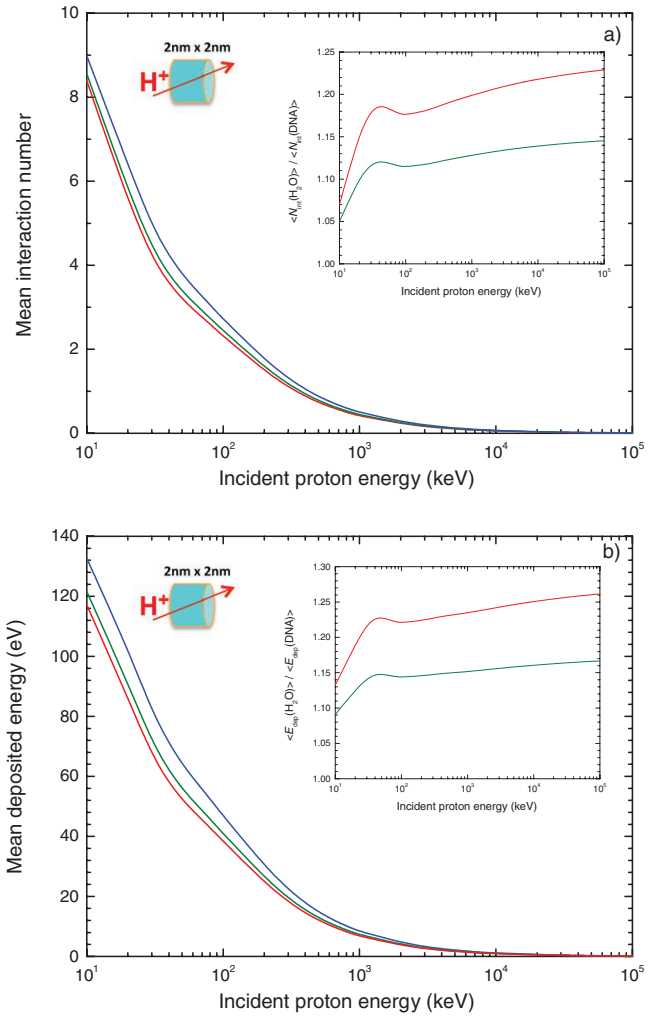

Figure 9. (Colour online) Mean number of ionizing interactions (panel a) and mean deposited energy (panel b) for proton-induced interactions in a DNA segment-size cylinder filled with water (blue line) or DNA (red line: dry DNA; green line: hydrated DNA). The density is equal to 1 g cm^{-3} in all cases.

to proton-irradiations may be either questionable or at least revised in the forthcoming MC track-structure codes. More importantly, we observed that the discrepancies between water and DNA (dry as well as hydrated) are not in the same ratio as the density (see inset of figure 9), which clearly demonstrates that a simple procedure of density rescaling is not able to reproduce the underlying physics of cellular irradiations.

Let us nevertheless remind that these results were obtained by assuming a water-equivalent density of 1 g cm^{-3} for the three media investigated. So, if a realistic density for DNA is used, namely, 1.29 g cm^{-3} for hydrated DNA (Birnie *et al* 1973) and 1.407 g cm^{-3} for dry DNA as reported by Smialek *et al* (2013), the previous results may be slightly revisited as reported in figure 10.

Thus, in the case of a realistic description of the biological medium (hydrated DNA), we observe that the energy transfers induced by proton impact in a critical DNA-segment cylinder volume is of about 15% higher than that observed if water is used in the simulation. This

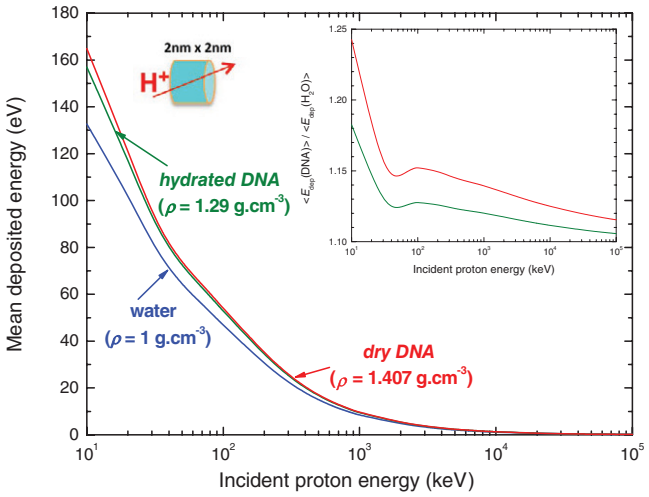

Figure 10. (Colour online) Mean deposited energy for proton-induced interactions in a DNA segment-size cylinder filled with water (blue line) or DNA (red line: dry DNA; green line: hydrated DNA). Realistic densities are used for the different media.

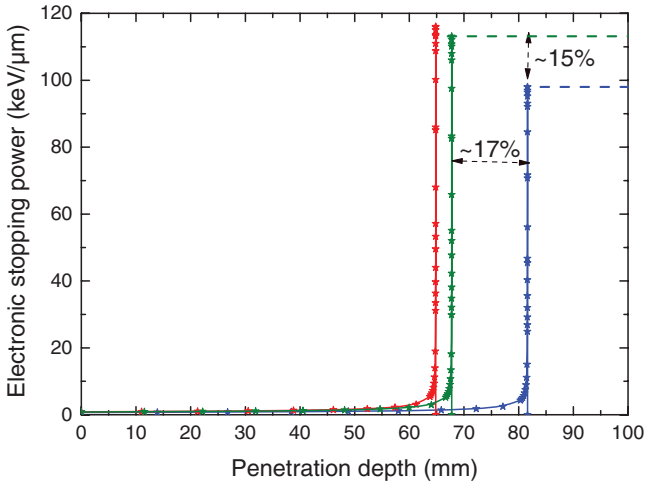

Figure 11. (Colour online) Bragg peak for 100 MeV proton beams in water (blue line) and DNA (red line: dry DNA; green line: hydrated DNA).

difference is particularly noticeable in the low-energy regime i.e. in the domain of predominance of the electron capture process ($E_i < 100$ keV). This finding is all the more important that this energy domain corresponds to the end part of the proton track in matter, namely, a region of prime interest in proton therapy since it corresponds to the maximum of energy deposit per path length. This specificity—referred as to the Bragg peak—is analysed in the following.

3.5. Radiotherapeutical endpoints

Comparatively to the photon case where most of the radiation is absorbed a few mm after the entrance of the radiation into the medium, the proton can cross a large distance before

stopping and then delivering its energy on-site. This charged-particle specificity is the basic concept of hadron therapy and more particularly of proton therapy where a maximal of efficiency (maximal of energy transfer) is required inside the tumour cell while sparing the surrounding healthy tissue. To illustrate this phenomenon, we commonly report the evolution of the stopping power versus the penetration depth of the projectile in the matter under consideration. Thus, it is clear that the above reported conclusions in terms of energy transfer underestimation when water is used as surrogate of the biological medium will undoubtedly lead to (i) a longer distance of penetration of the proton in the irradiated matter and (ii) an underestimation of the energy delivered to the tumour-site. Besides, it goes without saying the optimization of treatment planning is a far more complicated task and cannot be addressed by track structure simulations alone and requires the full understanding of a long sequence of events including physics, chemistry, biology and medicine as illustrated by the multi-scale approach provided by Solov'yov and co-workers [Solov'yov *et al* (2009) and Surdutovich and Solov'yov (2014)].

Figure 11 depicts the energy deposition distributions for a 100 MeV proton in the three media investigated in our study. We observe that using water instead of DNA clearly points out an overestimation of the penetration depth. More precisely, the Bragg peak is located at about 8.2 cm in the case of water whereas in the case of DNA medium, we found 6.8 cm and 6.5 cm for hydrated and dry DNA, respectively, that means a difference of about 17% in terms of localization. As regards the *absolute* value of energy deposit, an underestimation of about 15% is observed when water is used, namely 98 keV μm^{-1} for water versus 113 keV μm^{-1} for hydrated DNA.

4. Conclusions

Details on proton-induced collisions in living matter is of prime importance in many fields of medicine ranging from fundamental studies on DNA damage induction for radiobiology to refinement of treatment planning for better radiotherapy strategies in proton therapy. However, and although the use of (liquid) water as a tissue-equivalent medium is widely accepted in the majority of the existing numerical simulations, it remains an unsolved question whether this is the most relevant medium for radiobiological or radiotherapeutical studies.

In this context, we have here reported a detailed analysis of the main ionizing processes induced by proton-impact in water and on DNA components (both considered in vapour phase) including the nucleobases as well as the deoxyribose-phosphate group. Considerable differences in terms of cross sections were then reported for ionization as well as electron capture pointing out nevertheless the existence of a universal normalized cross section for both ionizing processes what suggested that using more 'realistic' cross sections instead of water ones would have no effect on the transport simulation of protons in biological medium. More importantly, we observed that the discrepancies between water and DNA (dry as well as hydrated) were not in the same ratio than their respective density, which clearly demonstrates that a simple procedure of density rescaling is not able to reproduce the underlying physics of cellular irradiations. In this context, a fine description of the various energy transfers induced by proton impact during both ionization and capture has pointed out strong discrepancies between water and DNA revealing also the crucial role of the sugar-phosphate backbone in particular when the electron capture process is scrutinized.

Finally, a realistic description of living matter has been proposed in order to evaluate at best the role played by the medium composition in the proton-induced energy deposit pattern and then to envisage a revision of the energy criteria commonly used for predicting the DNA double strand breakage.

The obtained results indicate that using cross sections of water vapour in track structure simulations leads to an underestimation of the proton-induced energetic cartography, that has relevant consequences on both radiation damage predictions and radiotherapeutical treatment planning as illustrated by a 100 MeV-proton Bragg peak profile.

The discrepancies also reported are all the more important that they underline that the approach commonly used in many Monte Carlo studies, which consists in rescaling the water vapour based track-structure simulations by a *realistic* density is clearly inappropriate for mimicking the biological reality.

Acknowledgments

The authors would like to thank the Mésocentre de Calcul Intensif Aquitain (MCIA, Bordeaux) and the University of Lorraine (Théorie-Modélisation-Simulation group, UMR CNRS 7565) for the free computer time provided. Besides, J M M, M E G, O A F, J H and R D R acknowledge financial support from the Agencia Nacional de Promoción Científica y Tecnológica through the project PICT 2011–2145 and from Consejo Nacional de Investigaciones Científicas y Técnicas through the project PIP 1026, both institutions from República Argentina. Finally, Sandia National Laboratories is a multi-program laboratory managed and operated by Sandia Corporation, a wholly owned subsidiary of Lockheed Martin Corporation, for the U.S. Department of Energy's National Nuclear Security Administration under contract DE-AC04-94AL85000.

References

Abril I, Garcia-Molina R, Denton C D, Kyriakou I and Emfietzoglou D 2011 energy loss of hydrogen- and helium-ion beams in DNA: calculations based on a realistic energy-loss function of the target *Radiat. Res.* **175** 247

Agnihotri A N *et al* 2012 Ionization of uracil in collisions with highly charged carbon and oxygen ions of energy 100 keV to 78 MeV *Phys. Rev.* A **85** 032711

Agnihotri A N, Nandi S, Kasthurirangan S, Kumar A, Galassi M E, Rivarola R D, Champion C and Tribedi L C 2013a Doubly differential distribution of electron emission in ionization of uracil in collisions with 3.5-MeV/u bare C ions *Phys. Rev.* A **87** 032716

Agnihotri A N *et al* 2013b Absolute total ionization cross sections of uracil ($C_4H_4N_2O_2$) in collisions with MeV energy highly charged carbon, oxygen and fluorine ions *J. Phys. B: At. Mol. Opt. Phys.* **46** 185201

Bernal M A, deAlmeida C E, Incerti S, Champion C, Ivanchenko V and Francis Z 2015 The influence of DNA configuration on the direct strand break yield *Comput. Math. Methods Med.* **2015** 417501

Bernal M A, Sikansi D, Cavalcante F, Incerti S, Champion C, Ivanchenko V and Francis Z 2013 An atomistic geometrical model of the B-DNA configuration for DNA-radiation interaction simulations *Comput. Phys. Comm.* **184** 2840–7

Bernhardt Ph and Paretzke H G 2003 Calculation of electron impact ionisation cross sections of DNA using the Deutsch-Märk and Binary-Encounter-Bethe formalisms *Int. J. Mass. Spectrom.* **223–224** 599

Birnie G D, Rickwood D and Hell A 1973 Buoyant densities and hydration of nucleic acids, proteins, and nucleoprotein complexes in metrizamide *Biochim. Biophys. Acta* **331** 283–94

Blanco S and Fournier R 2003 An invariance property of diffusive random walks *Europhys. Lett.* **61** 168–73

Bolorizadeh M A and Rudd M E 1986 Angular and energy dependence of cross sections for ejection electrons from water vapour. II. 15–150 keV proton impact *Phys. Rev.* A **33** 888–92

Champion C, Hanssen J and Rivarola R D 2013 *Theory of Heavy Ion Collision Physics in Hadron Therapy: Advances in Quantum Chemistry* 1st edn ed D Belkic vol 65 (Irvine, CA: Elsevier) p 269 Chap. 10

Champion C, Lekadir H, Galassi M E, Fójon O, Rivarola R D and Hanssen J 2010 Theoretical predictions for ionization cross sections of DNA nucleobases impacted by light ions *Phys. Med. Biol.* **55** 6053–67

Champion C, Weck P F, Lekadir H, Galassi M E, Fojón O, Abufager P, Rivarola R D and Hanssen J 2012 Proton-induced single electron capture on DNA/RNA bases *Phys. Med. Biol.* **57** 3039–49

Colson A O, Besler B and Sevilla M D 1993 *Ab initio* molecular orbital calculations on DNA radical ions. 3. Ionization potentials and ionization sites in components of the DNA sugar phosphate backbone *J. Phys. Chem.* **97** 8092

Corchs S E, Rivarola R D and McGuire J H 1993 Impact-parameter formulation for electron capture from molecular target *Phys. Rev.* A **47** 3937–44

Crothers D S F and McCann J F 1983 Ionisation of atoms by ion impact *J. Phys.* B **16** 3229

Dagnac R, Blanc D and Molina D 1970 A study on the collision of hydrogen H_1^+, H_2^+ and H_3^+ with a water-vapour target *J. Phys.* B*: At. Mol. Phys.* **3** 1239

Deng Z, Bald I, Illenberger E and Huels M A 2005 Beyond the Bragg Peak: hyperthermal heavy ion damage to DNA components *Phys. Rev. Lett.* **95** 153201

de Vera P, Abril I, Garcia-Molina R and Solov'yov A V 2013 Ionization of biomolecular targets by ion impact: input data for radiobiological applications *J. Phys: Conf. Ser.* **438** 012015

de Vera P, Garcia-Molina R and Abril I 2015 Angular and energy distributions of electrons produced in arbitrary biomaterials by proton impact *Phys. Rev. Lett.* **114** 018101

Dingfelder M 2014 Updated model for dielectric response function of liquid water *Appl. Radiat. Isot.* **83** 142–7

Emfietzoglou D, Kyriakou I, Garcia-Molina R, Abril I and Nikjoo H 2013 Inelastic cross sections for low-energy electrons in liquid water: exchange and correlation effects *Radiat. Res.* **180** 499–513

Friedland W, Dingfelder M, Kundrát and Jacob P 2011 Track structures, DNA targets and radiation effects in the biophysical Monte Carlo simulation code PARTRAC *Mut. Res.* **711** 28–40

Friedland W, Jacob P, Paretzke H G and Stork T 1998 Monte Carlo simulation of the production of short DNA fragments by low-linear energy transfer radiation using higher-order DNA models *Radiat. Res.* **150** 170

Frisch M J *et al* 2009 *Gaussian 09, Revision A.02* (Wallingford CT: Gaussian, Inc.)

Galassi M E, Champion C, Weck P F, Rivarola R D, Fojón O and Hanssen J 2012 Quantum-mechanical predictions of DNA and RNA ionization by energetic proton beams *Phys. Med. Biol.* **57** 2081–99

Galassi M E, Rivarola R D and Fainstein P D 2004 Multicenter character in single-electron emission from H_2 molecules by ion impact *Phys. Rev.* A **70** 032721

Gobet F, Farizon B, Farizon M, Gaillard M J, Carré M, Lezius M, Scheier P and Märk T D 2001 Total, partial, and electron-capture cross sections for ionization of water vapor by 20–150 keV protons *Phys. Rev. Lett.* **86** 3751

Goodhead D T, Leenhouts H P, Paretzke H G, Terrissol M, Nikjoo H and Blaauboer R 1994 Track structure approaches to the interpretation of radiation effects on DNA *Radiat. Prot. Dosim.* **52** 217–23

Hush N S and Cheung A S 1975 Ionization potentials and donor properties of nucleic acid bases and related compounds *Chem. Phys. Lett.* **34** 11

Iriki Y, Kikuchi Y, Imai M and Itoh A 2011a Absolute doubly differential cross sections for ionization of adenine by 1.0-MeV protons *Phys. Rev.* A **84** 032704

Iriki Y, Kikuchi Y, Imai M and Itoh A 2011b Proton-impact ionization cross sections of adenine measured at 0.5 and 2.0 MeV by electron spectroscopy *Phys. Rev.* A **84** 052719

Itoh A, Iriki Y, Imai M, Champion C and Rivarola R D 2013 Cross sections for ionization of uracil by MeV-energy proton impact *Phys. Rev.* A **88** 052711

Larkins F B 1977 Semiempirical Auger-electron energies for elements $10 \leqslant Z \leqslant 100$ *At. Data Nucl. Data Tables* **20** 313–87

La Verne J A and S M Pimblott 1995 Electron energy-loss distributions in solid, dry DNA *Radiat. Res.* **141** 208–87

Li Z, Cloutier P, Sanche L and Richard Wagner J 2010 Low-energy electron-induced DNA damage: effect of base sequence in oligonucleotide trimers *J. Am. Chem. Soc.* **132** 5422–7

Li Z, Zheng Y, Cloutier P, Sanche L and Richard Wagner J 2008 Low energy electron induced DNA damage: effects of terminal phosphate and base moieties on the distribution of damage *J. Am. Chem. Soc.* **130** 5612

Luna H *et al* 2007 Water-molecule dissociation by proton and hydrogen impact *Phys. Rev.* A **75** 042711

Martínez A E, Deco G R, Rivarola R D and Fainstein P D 1988 K-Shell vacancy production in asymmetric collisions *Nucl. Instrum. Methods Phys. Res.* B **34** 32–6
Nikjoo H 2003 Radiation track and DNA damage Iran *J. Radiat. Res.* **1** 3–16
Nikjoo H, Emfietzoglou D, Watanabe R and Uehara S 2008 Can Monte Carlo track structure codes reveal reaction mechanism in DNA damage and improve radiation therapy? *Radiat. Phys. Chem.* **77** 1270
Nikjoo H, Martin R F, Charlton D E, Terrissol M, Kandaiya P and Lobachevsky P 1996 Modelling of Auger-induced DNA damage by incorporated 125I *Acta Oncol.* **35** 849–56
Nikjoo H, O'Neill P, Terrissol M and Goodhead D T 1999 Quantitative modelling of DNA damage using Monte Carlo track structure method *Radiat. Environ. Biophys.* **38** 31–8
Nikjoo H, Uehara S, Emfietzoglou D and Cucinotta F A 2006 Track-structure codes in radiation research *Radiat. Meas.* **41** 1052
Pater P, Seuntjens J, El Naqa I, and Bernal M A 2014 On the consistency of Monte Carlo track structure DNA damage simulations *Med. Phys.* **41** 121708
Privett A J and Morales J A 2014 Electron nuclear dynamics of proton collisions with DNA/RNA bases at $E_{\mathrm{Lab}} = 80$ keV: a contribution to proton cancer therapy research *Chem. Phys. Lett*. **603** 82–8
Rabus H *et al* 2014 Biologically weighted quantities in radiotherapy: an EMRP joint research project *EPJ Web Conf.* **77** 00021
Rivarola R D, Galassi M E, Fainstein P D and Champion C 2013 *Theory of Heavy Ion Collision Physics in Hadron Therapy: Advances in Quantum Chemistry* 1st edn ed D Belkic vol 65 (Irvine, CA: Elsevier) p 231 Chap. 9
Rudd M E, Goffe T V, DuBois R D and Toburen L H 1985 Cross sections for ionization of water vapour by 7–4000 keV protons *Phys. Rev.* A **31** 492–4
Siegbahn H, Asplund L and Kelfve P 1975 The auger electron spectrum of water vapour *Chem. Phys. Lett.* **35** 330–5
Smialek M, Jones N C and Vrønning Hoffmann S 2013 Measuring the density of DNA films using ultraviolet-visible interferometry *Phys. Rev.* E **87** 060701
Solov'yov A V, Surdutovich E, Scifoni E, Mishustin I and Greiner W 2009 Physics of ion beam cancer therapy: a multiscale approach *Phys. Rev.* E **79** 011909
Surdutovich E and Solov'yov A V 2014 Multiscale approach to the physics of radiation damage with ions *Eur. Phys. J.* D **68** 353
Tabet J, Eden S, Feil S, Abdoul-Carime H, Farizon B, Farizon M, Ouaskit S and Märk T D 2010 Absolute total and partial cross sections for ionization of nucleobases by proton impact in the Bragg peak velocity range *Phys. Rev.* A **82** 022703
Tan Z, Xia Y, Zhao M and Liu X 2006 Proton stopping power in a group of bioorganic compounds over the energy range of 0.05–10 MeV *Nucl. Instrum. Methods* B **248** 1–6
Toburen L H 1998 Ionization and charge-transfer: basic data for track structure calculations *Radiat. Env. Biophys.* **37** 221
Yokoya A, Cunniffe S M T and O'Neill P 2002 Effect of hydration on the induction of strand breaks and base lesions in plasmid DNA films by γ-radiation *J. Am. Chem. Soc.* **124** 8859–66
Zheng Y, Cloutier P, Hunting D J, Sanche L and Richard Wagner J 2005 Chemical basis of DNA sugar-phosphate cleavage by low-energy electrons *J. Am. Chem. Soc.* **127** 16592